NANO LETTERS

LETTER

pubs.acs.org/NanoLett

Nanomechanical Membrane-type Surface Stress Sensor

Genki Yoshikawa,*,† Terunobu Akiyama,‡ Sebastian Gautsch,‡ Peter Vettiger,‡ and Heinrich Rohrer§

†World Premier International (WPI) Research Center, International Center for Materials Nanoarchitectonics (MANA), National Institute for Materials Science (NIMS), 1-1 Namiki, Tsukuba, Ibaraki 305-0044, Japan

‡Institute of Microengineering (IMT), Ecole Polytechnique Fédérale de Lausanne (EPFL), Jaquet-Droz 1, Neuchâtel CH-2002, Switzerland

§Wollerau CH-8832, Switzerland

Supporting Information

ABSTRACT: Nanomechanical cantilever sensors have been emerging as a key device for real-time and label-free detection of various analytes ranging from gaseous to biological molecules. The major sensing principle is based on the analyte-induced surface stress, which makes a cantilever bend. In this letter, we present a membrane-type surface stress sensor (MSS), which is based on the piezoresistive read-out integrated in the sensor chip. The MSS is not a simple "cantilever," rather it consists of an "adsorbate membrane" suspended by four piezoresistive "sensing beams," composing a full Wheatstone bridge. The whole analyte-induced isotropic surface stress on the membrane is efficiently transduced to the piezoresistive beams as an amplified uniaxial stress. Evaluation of a prototype MSS used in the present experiments demonstrates a high sensitivity which is comparable with that of optical methods and a factor of more than 20 higher than that obtained with a standard piezoresistive cantilever. The finite element analyses indicate that changing dimensions of the membrane and beams can substantially increase the sensitivity further. Given the various conveniences and advantages of the integrated piezoresistive read-out, this platform is expected to open a new era of surface stress-based sensing.

KEYWORDS: Piezoresistive, surface stress, finite element analysis (FEA), microcantilever, integration, optimization

Nanomechanical cantilever array sensors[1−3] have been attracting a wide range of attention because of their various advantages, such as real-time and label-free detection of minute amounts of materials. Various applications have been demonstrated using cantilever array sensors, including electrical nose[4] and chemical and biological detection.[5−12] The surface of a cantilever is coated by a receptor layer on which the target molecules adsorb or react. In the static mode, the adsorbates-induced surface stress makes the cantilever bend, while in the dynamic mode the adsorbates change the resonance frequency of a cantilever due to mass loading. In the present investigations, we deal with the static mode. Since surface stress emerges not only with the adsorption of molecules but also with the nanomechanical structural changes of substances on the surface, the scope of the surface stress-based sensing can cover various phenomena.[13,14]

Most studies employ optical detection of the cantilever deflection in both modes.[1−13] This approach, however, causes several practical problems for actual applications, for example, bulky, time-consuming laser alignment on each cantilever, low applicability for large one- or two-dimensional arrays, and the difficulty of performing measurements in opaque liquids, such as blood. One of the most promising solutions to these problems is a use of lever-integrated piezoresistive sensing,[14−25] which does not require bulky and complex peripheries related with an optical read-out and can be used for the detection in any opaque liquid with large multidimensional arrays. It is worth noting that the compact atomic force microscope (AFM) with integrated piezoresistive cantilevers was loaded on the Phoenix Mars Lander conducted by National Aeronautics and Space Administration (NASA) and succeeded in the first nanometer identification of extraterrestrial soil on the Mars.[19−21] Despite these inherent advantages, piezoresistive cantilevers have not been widely in use for adsorbate-induced surface stress sensing applications. The reason is that, without effective mechanical amplification schemes, their sensitivity is far below that of optical methods.

To address the appropriate scheme for the sensitivity enhancement of the piezoresistive cantilever sensors, we briefly review the basic properties of a piezoresistive cantilever for surface stress sensing. We focus on p-type piezoresistors created by boron diffusion onto a single-crystal Si with (100) surface to take advantage of its high piezocoefficient.[26−28] Assuming plain stress (i.e., $\sigma_z = 0$), relative resistance change can be described as follows[28,29]

$$\frac{\Delta R}{R} \approx \frac{1}{2}\pi_{44}(\sigma_x - \sigma_y) \qquad (1)$$

where π_{44} ($\sim 138.1 \times 10^{-11}$ Pa^{-1}) is one of the fundamental piezoresistance coefficients of the silicon crystal. σ_x, σ_y, and σ_z are stresses induced on the piezoresistor in [110], [1-10], and [001] directions of the crystal, respectively. According to eq 1,

Received: November 5, 2010

   dx.doi.org/10.1021/nl103901a | *Nano Lett.* XXXX, XXX, 000–000

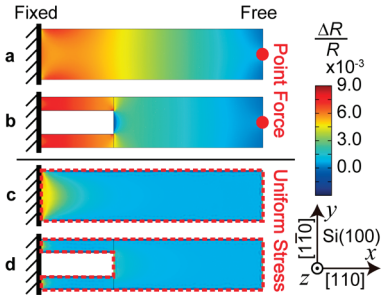

Figure 1. Distribution of $\Delta R/R$ on the surface of cantilevers with and without constriction calculated by finite element analyses (FEA) using COMSOL Multiphysics 3.5a. The direction of current flow is assumed to be in x-direction. (a,b) A point force is applied at the free end (red filled circle position). (c,d) A compressive surface stress (-3.0 N/m) is applied uniformly on the whole surface surrounded by red dashed lines, resulting in downward deflection and tensile stresses ($+\sigma_x$ and $+\sigma_y$) inside the cantilever from the top surface to the neutral line. Piezoresistors are supposed to be embedded inside the cantilever near to the top surface. Dimension of all cantilevers is $135 \times 30 \times 1\ \mu m^3$, while that of the constricted parts in (b,d) consist of two parts of $45 \times 8 \times 1\ \mu m^3$. Thus, the total area of the piezoresistors placed at these constricted parts is $90 \times 8\ \mu m^2$. The deflection of the free ends of the cantilevers is the same (~700 nm, downward) in all cases.

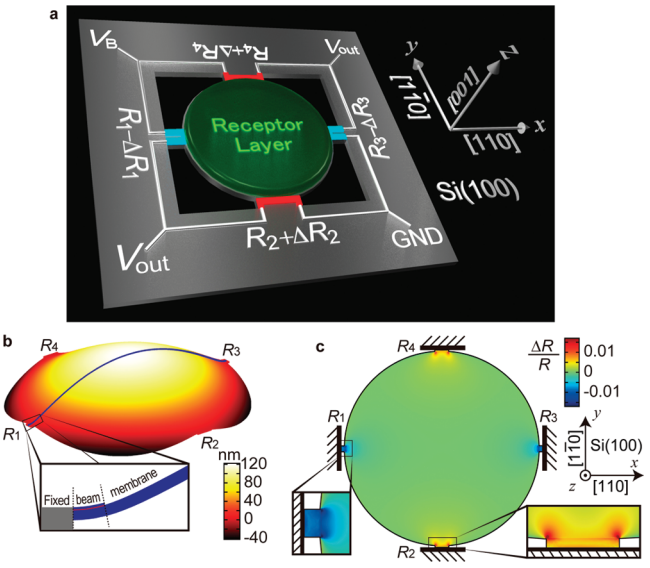

Figure 2. (a) Schematic illustration of the MSS with p-type piezoresistors on n-type single crystal Si(100). In this configuration with current flowing in x-direction, blue- (R_1 and R_3) and red (R_2 and R_4) colored piezoresistors give opposite signs in $\Delta R/R$ in response to the surface stress induced on the adsorbate membrane because σ_x and σ_y are dominant in those piezoresistors, respectively (cf. eq 1). (b,c) FEA results for the MSS with a compressive surface stress of -3.0 N/m applied uniformly on the adsorbate membrane, resulting in dominant stresses of $-\sigma_x$ and $-\sigma_y$ on R_1, R_3 and R_2, R_4, respectively. (b) Deformed shape of the MSS. (Inset) Magnified image of the cross section along the blue line, and the red-colored part indicates the embedded piezoresistor. Note that the deformed shape is exaggerated by 500 times. (c) Distribution of $\Delta R/R$ on the surface of MSS with current flowing in x-direction. (Insets) Magnified images of the sensing beams for R_1 and R_2. Dimensions of each part in direction $x \times y \times z$ are as follows; adsorbate membrane: (ϕ500) $\times$ 3.2 μm^3; sensing beams for R_1, R_3, $10 \times 16 \times 3.2\ \mu m^3$; for R_2, R_4, $36 \times 5 \times 3.2\ \mu m^3$. All of the sensing beams are covered by silicon oxide (0.6 μm) and silicon nitride (0.1 μm) layers.

both enhancement of σ_x (σ_y) and suppression of σ_y (σ_x) are required to yield a substantial amount of $\Delta R/R$.

The piezoresistive detection for surface stress sensing requires very different approaches from those for force sensing applications, such as AFM. In the case of force loading (Figure 1a,b; e.g., for AFM), the induced stress on the surface is uniaxial and increases from zero at the free end to maximum at the clamped end. The stress at the clamped end is readily amplified by a constriction.[15] Thus, the piezoresistors embedded at the constricted parts can yield larger signal. In the case of adsorbate-induced surface stress loading (Figure 1c,d), the stress is, however, isotropic and the piezoresistive signal is virtually zero except at the clamped end where the isotropic symmetry is broken. σ_x recovers its full value at a distance of the order of the cantilever thickness, while σ_y remains reduced up to a distance comparable to the width of the lever.[29] Thus the largest piezoresistive signal is measured close to the clamped end but drops to zero at the distances about the width of the lever from the clamped end.

There are several reports on the improvement of the sensitivity of piezoresistive cantilevers for surface stress sensing applications by structural modification, such as making a through hole,[30,31] patterning of the cantilever surface,[32] or variation of geometrical parameters (e.g., length, width, and overall shapes).[33,34] Since all of these approaches rely on suppressing one of the isotropic stress components, they have not yielded significant stress amplification to make piezoresistive detection comparable to the optical approach.

Taking account of this intrinsic problem, analytical consideration of strain amplification schemes for sensing applications[35] based on the strategies of the constriction and double lever geometries[35,36] has led us to a membrane-type surface stress sensor (MSS). Figure 2a shows the basic configuration of the MSS consisting of an "adsorbate membrane" supported with four constrictions, "sensing beams," on which piezoresistors are embedded. Although isotropic surface stress leads to zero piezoresistive signal owing to eq 1, it causes an isotropic deformation. The concept of the MSS structure is based on an effective conversion of the isotropic deformation, which is accumulated at the periphery of the membrane, into a force at the connection between the membrane and the small sensing beams. With this configuration, each sensing beam experiences the cumulative deformation of the membrane and, thus, piezoresistors embedded at these sensing beams can efficiently detect the whole surface stress applied on the adsorbate membrane. Figure 2b shows the deformation of the membrane caused by the adsorbate-induced uniform and isotropic compressive surface stress (-3.0 N/m; same as Figure 1c,d) calculated by FEA for a MSS with a diameter of 500 μm. Here we define compressive and tensile stresses as negative and positive values, respectively. The uniform compressive surface stress induces circular deflection of the membrane, resulting in the concave downward shape of the membrane and making all sensing beams deflect upward (Figure 2b). It should be noted that contrary to a "cantilever" the compressive (tensile) surface stress on the upper surface of the membrane leads to the compressive (tensile) stress on the piezoresistors placed on the upper side of the sensing beams as presented in the inset of Figure 2b, resulting in dominant stresses of $-\sigma_x$ ($+\sigma_x$) and $-\sigma_y$ ($+\sigma_y$) on R_1, R_3 and R_2, R_4, respectively. While the round membrane yields similar output signals with other shapes (e.g., square or rhombus) with a few percent differences according to FEA, it can provide several practical

dx.doi.org/10.1021/nl103901a |*Nano Lett.* XXXX, XXX, 000–000

advantages, such as an easy coating with liquid solution using inkjet spotting method or a better sample flow with a wider opening around the membrane.

The membrane-type geometry allows configuring a full Wheatstone bridge to enhance the signal further, exploiting the single crystal property of silicon. In case all four resistors ($R_1 \sim R_4$) are practically equal and that the relative resistance changes are small with $\Delta Ri/Ri << 1$ ($i = 1 \sim 4$), the total output signal V_{out} can be approximated by

$$V_{out} = \frac{V_B}{4}\left(\frac{\Delta R_1}{R_1} - \frac{\Delta R_2}{R_2} + \frac{\Delta R_3}{R_3} - \frac{\Delta R_4}{R_4}\right) \quad (2)$$

Thus, if the signs of the resistance changes ΔR_1 and ΔR_3 are opposite to those of ΔR_2 and ΔR_4, the full Wheatstone bridge yields an amplification of another factor of four. Taking into account the single crystal property of p-type Si(100), the relative resistance changes of four resistors with the configuration shown in Figure 2a with a current flow in x-direction are all given by eq 1.[27] The dominant stresses induced by surface stress on the adsorbate membrane are σ_x in R_1, R_3 and σ_y in R_2, R_4, resulting in opposite signs for the relative resistance changes in each set of resistors. Thus, all sensing beams effectively contribute to the total output signal of MSS.

For quantitative comparison with the standard cantilever, the averaged values of relative resistance change ($\Delta R/R|_{ave}$) on the piezoresistive parts (sensing beams in the MSS and two "legs" in the standard cantilever) are calculated as follows

$$\left.\frac{\Delta R}{R}\right|_{ave} = \frac{1}{A_R}\int_0^{A_R}\frac{\Delta R}{R}\,dA \quad (3)$$

where A_R is the area of a piezoresistor. The calculated values of the resistors in each beam are $\Delta R_1/R_1|_{ave} = \Delta R_3/R_3|_{ave} = -9.39 \times 10^{-3}$ and $\Delta R_2/R_2|_{ave} = \Delta R_4/R_4|_{ave} = 6.55 \times 10^{-3}$, yielding $\Delta R/R|_{ave} = 3.19 \times 10^{-2}$ in total with a full Wheatstone bridge. It is ~43 times higher value compared to that of the standard cantilever presented in Figure 1d ($\Delta R/R|_{ave} = 7.41 \times 10^{-4}$).

We have fabricated an array of MSS (Figure 3). Two sizes of a membrane having diameters of 500 and 300 μm were fabricated in a same array (Figure 3a). The dimensions of sensing beams and passivation layers of the MSS are same as those presented in Figure 2b,c. The standard cantilever having the same dimension with that presented in Figure 1d was also examined for comparison.

The membranes and the standard cantilever were both coated with polyethyleneimine (PEI) layers by an inkjet spotting method. These specimens were exposed to 20% water vapor in pure nitrogen carrier gas with a flow rate of 100 mL/min for 5 min. Three cycles with intervals of 5 min for nitrogen purging have been executed. Figure 3b shows the obtained output signal (V_{out}) of the MSS and the standard cantilever. Both signals were measured with the same electrical setup with a bias voltage of −1.5 V in both cases. The 500 and 300 μm membranes exhibited respectively ~22 and ~15 times higher signals than that of the standard cantilever. This experimental result confirms a significantly enhanced sensitivity as well as its membrane size dependence which is described in the next paragraph. The discrepancy from the FEA is presumably due to several neglected parameters in calculations, such as diffusion depth of the dopant, surface profile caused by etching process, or difference in uniformity of the coating layers. We obtained the enhancement

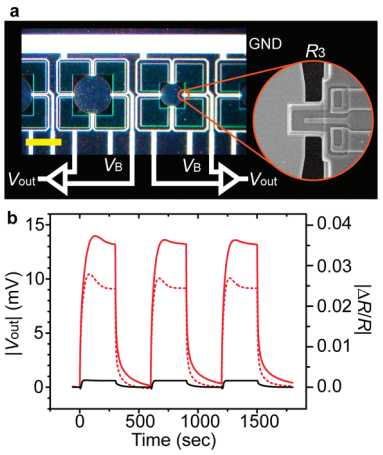

Figure 3. (a) Photograph of the fabricated MSS array chip with a schematics of a part of electrical connections. (Inset) Magnified scanning electron microscope (SEM) image of the piezoresistive sensing beam (R_3). MSS with two different diameters of 500 and 300 μm are fabricated in a same array. Yellow scale bar corresponds to 500 μm. (b) Obtained output signal (V_{out}). The signal from the MSS with diameters of 500 and 300 μm are plotted with red solid and dashed lines, while that from the standard cantilever is plotted with a black line.

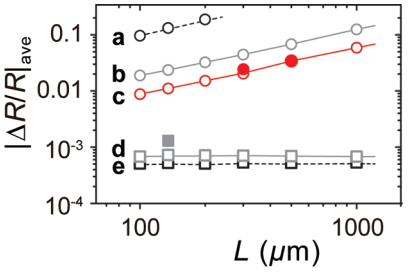

Figure 4. Dependence of the averaged relative resistance changes ($|\Delta R/R|_{ave}$) on L (diameter of the adsorbate membrane for MSS (a−c; circles); length of the standard cantilever with a width of 30 μm (d,e; squares)). Open symbols represent the results obtained by FEA, and the filled ones indicate the experimental results. For the MSS, the dimensions of the sensing beams are fixed as follows: for R_1 and R_3, $5 \times 4 \times 1$ μm^3, $45 \times 16 \times 1$ μm^3, and $10 \times 16 \times 3.2$ μm^3 (on which two piezoresistors with half beam width are placed in series forming "U"-shape (cf. Figure 2a)); for R_2 and R_4, $10 \times 2 \times 1$ μm^3, $90 \times 8 \times 1$ μm^3, and $36 \times 5 \times 3.2$ μm^3; for lines a, b, and c, respectively. For the standard cantilever, the dimensions of the two legs each are fixed as follows: $5 \times 2 \times 1$ μm^3, $45 \times 8 \times 1$ μm^3 for lines d and e, respectively. Thus, each piezoresistor is set at the same dimensions for gray (90×8 μm^2; b,d) and dashed (10×2 μm^2; a,e) lines.

in sensitivity even with rather thicker membrane and sensing beams (3.2 μm) of MSS compared to that of the standard cantilever (1−1.5 μm). While the overall performance depends also on the dimensions and properties of piezoresistors and passivation layers, the reduction in thickness leads to an almost linear increase in sensitivity according to FEA. Thereby, a MSS having the same thickness with similar passivation layers as that of the standard cantilever (50 nm of silicon nitride film) can gain another 2−3 times amplification in sensitivity.

Another important difference between a MSS and a standard cantilever is the size dependence on a signal. Since the analyte-induced surface stress can be efficiently transduced at the piezoresistive sensing beams in the MSS geometry, a larger

dx.doi.org/10.1021/nl103901a |Nano Lett. XXXX, XXX, 000–000

Table 1. Comparison between an Optical Read-out (a) and the Piezoresistive Read-out Methods with the MSS (b,c) and the Standard Piezoresistive Cantilever (d)[a]

type	dimension (μm × μm × μm)	area of piezoresistors (μm × μm)	signal by surface stress of −3.0 N/m; S	experimental noise; N	S/N	minimum detectable surface stress (mN/m)
(a) optical	500 × 100 × 1		9950 nm	0.5−3.0 nm	3320−19900	0.15−0.90
(b) MSS (Exp)	(ϕ500) × 3.2	20 × 3.8	13100 μV	1.0−1.5 μV	8730−13100	0.23−0.34
(c) MSS	(ϕ1000) × 1	90 × 8	47300 μV	1.0−1.5 μV	31500−47300	0.095−0.063
(d) stand CL (Exp)	135 × 30 × 1	90 × 8	598 μV	1.0−1.5 μV	399−598	5.0−7.5

[a] The values of (b,d) are obtained by the experiments, while those of (a,c) are simulated by FEA. S/N corresponds to the signal-to-noise ratio at the surface stress of −3.0 N/m with the experimental noises (N).

adsorbate membrane or smaller sensing beams lead to a larger resistance change, that is, higher sensitivity. Figure 4 shows the size dependence on relative resistance changes of various geometries. Each piezoresistor is set at the same dimensions for gray (90 × 8 μm^2; b,d) and dashed (10 × 2 μm^2; a,e) lines in Figure 4. The size dependence can be clearly seen for the MSS geometries (lines a−c with circle symbols), whereas standard cantilevers result in almost constant value of $|\Delta R/R|$ irrespective of its dimensions (lines d,e with square symbols). The larger aspect ratio between beams and membrane can achieve the larger enhancement in MSS because of the constriction effects,[35] whereas there is almost no dependence for the standard cantilever architecture.

Finally, we compare the performance of the MSS structures with common optically read-out cantilever sensors. Table 1 shows the signal-to-noise ratio and minimum detectable surface stress of an optical read-out system with a cantilever having a typical dimension (500, 100, and 1 μm in length, width, and thickness; Table 1a) and the piezoresistive read-out methods with the MSS (Table 1b,c) and standard cantilever (Table 1d). The signals are based on the surface stress of −3.0 N/m, which is evaluated by FEA based on the actually measured signal of the MSS in the experiments shown in Figure 3. The values in Table 1b,d are experimentally obtained, while those in Table 1a,c are calculated by FEA. The experimental noise (N) is based on the typical values reported in previous studies with a sample flow; for the optical read-out,[4,6−11] 0.5−3 nm (Table 1a), and for piezoresistive read-out (Table 1b−d), 1.0−1.5 μV, which is the actually recorded noise level arising from an electrical circuit at the present measurements in Figure 3. The intrinsic noises (Johnson (thermal) and Hooge (1/f) noises) in the piezoresistors are estimated to be lower than this experimental noise level (see Supporting Information for details). It is confirmed that the MSS has comparable sensitivity to the optical read-out methods with the experimentally demonstrated prototype chip shown in Figures 2 and 3 (Table 1b), while the standard piezoresistive cantilever (Table 1d) is one or 2 orders of magnitude less sensitive than the optical read-out as is consistent with the common observations. As shown in Table 1c for an example, the MSS structure has a potential for further enhancement in sensitivity up to several orders of magnitude by changing the dimensions of the adsorbate membrane and sensing beams although an effective amplification would be somewhat reduced because of practical requirements, such as properties of piezoresistors or passivation layers on the sensing beams.

In conclusion, we have presented a new type of nanomechanical sensor, namely MSS. The MSS allows concentrating the analyte-induced isotropic surface stress on the membrane at the four piezoresistive sensing beams composing a full Wheatstone bridge. Experimental measurements using the MSS have demonstrated a high sensitivity that is comparable with that of the optical methods. According to FEA, further substantial enhancement in sensitivity is expected by changing the dimensions of the MSS. Although we started to explore a structure to improve the sensitivity of a piezoresistive "cantilever," comprehensive analyses and simulations have brought us to the conclusion of a "non-cantilever" structure. Considering the significant improvement in sensitivity and the advantages gained by the integrated piezoresistive sensing, the MSS and its array structure will open a new era of the surface stress-based sensing.

■ ASSOCIATED CONTENT

Supporting Information. Details of finite element analyses, microfabrication procedure of the MSS, surface coating by an inkjet spotting method, vapor flow measurements, and evaluation of the intrinsic noise level for piezoresistive read-out. This material is available free of charge via the Internet at http://pubs.acs.org.

■ AUTHOR INFORMATION

Corresponding Author

*Tel: +81 (0) 29-851-3354 (ext. 8908). Fax: +81 (0) 29-860-4828. E-mail: YOSHIKAWA.Genki@nims.go.jp.

■ ACKNOWLEDGMENT

We express our appreciation to Professor Masakazu Aono and Dr. Tomonobu Nakayama from International Center for Materials Nanoarchitectonics (MANA), National Institute for Materials Science (NIMS), Tsukuba, Japan and Professor Nicolaas de Rooij from Institute of Microengineering (IMT) of Ecole Polytechnique Fédérale de Lausanne (EPFL), Neuchatel, Switzerland, for their help and support. We acknowledge the technical support by the staff of Comlab, the CSEM micro- and nanofabrication facility. This research was supported by World Premier International Research Center (WPI) Initiative on Materials Nanoarchitronics and by the Grant-in-Aid for Young Scientist (B) 21750083 (2009), MEXT, Japan.

■ REFERENCES

(1) Barnes, J. R.; Stephenson, R. J.; Welland, M. E.; Gerber, C.; Gimzewski, J. K. *Nature* **1994**, *372*, 79.

(2) Gimzewski, J. K.; Gerber, C.; Meyer, E.; Schlittler, R. R. *Chem. Phys. Lett.* **1994**, *217*, 589.

(3) Thundat, T.; Warmack, R. J.; Chen, G. Y.; Allison, D. P. *Appl. Phys. Lett.* **1994**, *64*, 2894.

(4) Lang, H. P.; Baller, M. K.; Berger, R.; Gerber, C.; Gimzewski, J. K.; Battiston, F. M.; Fornaro, P.; Ramseyer, J. P.; Meyer, E.; Guntherodt, H. J. *Anal. Chim. Acta* **1999**, *393*, 59.
(5) Berger, R.; Delamarche, E.; Lang, H. P.; Gerber, C.; Gimzewski, J. K.; Meyer, E.; Guntherodt, H. J. *Science* **1997**, *276*, 2021.
(6) Fritz, J.; Baller, M. K.; Lang, H. P.; Rothuizen, H.; Vettiger, P.; Meyer, E.; Guntherodt, H. J.; Gerber, C.; Gimzewski, J. K. *Science* **2000**, *288*, 316.
(7) McKendry, R.; Zhang, J. Y.; Arntz, Y.; Strunz, T.; Hegner, M.; Lang, H. P.; Baller, M. K.; Certa, U.; Meyer, E.; Guntherodt, H. J.; Gerber, C. *Proc. Natl. Acad. Sci. U.S.A.* **2002**, *99*, 9783.
(8) Backmann, N.; Zahnd, C.; Huber, F.; Bietsch, A.; Pluckthun, A.; Lang, H. P.; Guntherodt, H. J.; Hegner, M.; Gerber, C. *Proc. Natl. Acad. Sci. U.S.A.* **2005**, *102*, 14587.
(9) Zhang, J.; Lang, H. P.; Huber, F.; Bietsch, A.; Grange, W.; Certa, U.; McKendry, R.; Güntherodt, H.-J.; Hegner, M.; Gerber, C. *Nat. Nanotechnol.* **2006**, *1*, 214.
(10) Watari, M.; Galbraith, J.; Lang, H. P.; Sousa, M.; Hegner, M.; Gerber, C.; Horton, M. A.; McKendry, R. A. *J. Am. Chem. Soc.* **2007**, *129*, 601.
(11) Ndieyira, J. W.; Watari, M.; Barrera, A. D.; Zhou, D.; Vogtli, M.; Batchelor, M.; Cooper, M. A.; Strunz, T.; Horton, M. A.; Abell, C.; Rayment, T.; Aeppli, G.; McKendry, R. A. *Nat. Nanotechnol.* **2008**, *3*, 691.
(12) Raorane, D. A.; Lim, M. D.; Chen, F. F.; Craik, C. S.; Majumdar, A. *Nano Lett.* **2008**, *8*, 2968.
(13) Ghatkesar, M. K.; Lang, H. P.; Gerber, C.; Hegner, M.; Braun, T. *PLoS One* **2008**, *3*, e3610.
(14) Mukhopadhyay, R.; Sumbayev, V. V.; Lorentzen, M.; Kjems, J.; Andreasen, P. A.; Besenbacher, F. *Nano Lett.* **2005**, *5*, 2385.
(15) Tortonese, M.; Barrett, R. C.; Quate, C. F. *Appl. Phys. Lett.* **1993**, *62*, 834.
(16) Yoshikawa, G.; Lang, H. P.; Akiyama, T.; Aeschimann, L.; Staufer, U.; Vettiger, P.; Aono, M.; Sakurai, T.; Gerber, C. *Nanotechnology* **2009**, *20*, No. 015501.
(17) Aeschimann, L.; Meister, A.; Akiyama, T.; Chui, B. W.; Niedermann, P.; Heinzelmann, H.; De Rooij, N. F.; Staufer, U.; Vettiger, P. *Microelectron. Eng.* **2006**, *83*, 1698.
(18) Arlett, J. L.; Maloney, J. R.; Gudlewski, B.; Muluneh, M.; Roukes, M. L. *Nano Lett.* **2006**, *6*, 1000.
(19) Akiyama, T.; Gautsch, S.; de Rooij, N. F.; Staufer, U.; Niedermann, P.; Howald, L.; Muller, D.; Tonin, A.; Hidber, H. R.; Pike, W. T.; Hecht, M. H. *Sens. Actuators, A* **2001**, *91*, 321.
(20) Gautsch, S.; Akiyama, T.; Imer, R.; de Rooij, N. F.; Staufer, U.; Niedermann, P.; Howald, L.; Brandlin, D.; Tonin, A.; Hidber, H. R.; Pike, W. T. *Surf. Interface Anal.* **2002**, *33*, 163.
(21) Hecht, M. H.; Marshall, J.; Pike, W. T.; Staufer, U.; Blaney, D.; Braendlin, D.; Gautsch, S.; Goetz, W.; Hidber, H. R.; Keller, H. U.; Markiewicz, W. J.; Mazer, A.; Meloy, T. P.; Morookian, J. M.; Mogensen, C.; Parrat, D.; Smith, P.; Sykulska, H.; Tanner, R. J.; Reynolds, R. O.; Tonin, A.; Vijendran, S.; Weilert, M.; Woida, P. M. *J. Geophys. Res., [Planets]* **2008**, 113.
(22) Boisen, A.; Thundat, T. *Mater. Today* **2009**, *12*, 32.
(23) Thaysen, J.; Boisen, A.; Hansen, O.; Bouwstra, S. *Sens. Actuators, A* **2000**, *83*, 47.
(24) Lutwyche, M.; Andreoli, C.; Binnig, G.; Brugger, J.; Drechsler, U.; Haberle, W.; Rohrer, H.; Rothuizen, H.; Vettiger, P.; Yaralioglu, G.; Quate, C. *Sens. Actuators, A* **1999**, *73*, 89.
(25) Hierlemann, A.; Lange, D.; Hagleitner, C.; Kerness, N.; Koll, A.; Brand, O.; Baltes, H. *Sens. Actuators, B* **2000**, *70*, 2.
(26) Kanda, Y. *IEEE Trans. Electron Devices* **1982**, *29*, 64.
(27) Pfann, W. G.; Thurston, R. N. *J. Appl. Phys.* **1961**, *32*, 2008.
(28) Kanda, Y. *Sens. Actuators, A* **1991**, *28*, 83.
(29) Rasmussen, P. A.; Hansen, O.; Boisen, A. *Appl. Phys. Lett.* **2005**, *86*, 203502.
(30) He, J. H.; Li, Y. F. *J. Phys. (Paris)* **2006**, *34*, 429.
(31) Yu, X. M.; Tang, Y. Q.; Zhang, H. T.; Li, T.; Wang, W. *IEEE Sens. J.* **2007**, *7*, 489.
(32) Privorotskaya, N. L.; King, W. P. *Microsyst. Technol.* **2008** *15*, 333.
(33) Goericke, F. T.; King, W. P. *IEEE Sens. J.* **2008**, *8*, 1404.
(34) Loui, A.; Goericke, F. T.; Ratto, T. V.; Lee, J.; Hart, B. R.; King, W. P. *Sens. Actuators, A* **2008**, *147*, 516.
(35) Yoshikawa, G.; Rohrer, H. 7th International Workshop on Nanomechanical Cantilever sensor, Banff, Alberta, May 26−28, 2010.
(36) Yang, S. M.; Yin, T. I.; Chang, C. *Sens. Actuators, B* **2007**, *121*, 545.

dx.doi.org/10.1021/nl103901a |*Nano Lett.* XXXX, XXX, 000–000